Biosensors and Bioelectronics 31 (2012) 105–109

Contents lists available at SciVerse ScienceDirect

Biosensors and Bioelectronics

journal homepage: www.elsevier.com/locate/bios

Ultra-sensitive suspended graphene nanocomposite cancer sensors with strong suppression of electrical noise

Bo Zhang, Qiao Li, Tianhong Cui*

Department of Mechanical Engineering, University of Minnesota, 111 Church Street S.E., Minneapolis, MN 55455, USA

ARTICLE INFO

Article history:
Received 4 September 2011
Received in revised form
28 September 2011
Accepted 29 September 2011
Available online 6 October 2011

Keywords:
Graphene
Suspended beam
Self-assembly
Electrical noise
Cancer sensor

ABSTRACT

The cancer sensor based on suspended layer-by-layer self-assembled graphene reported in the paper exhibits an ultra high sensitivity due to graphene material properties in nature. By simply immersing the substrate alternatively into charged graphene suspensions and polyions, graphene nanoplatelets are self-assembled in the channel as the sensing region, followed by SF_6 dry etching to suspend the structure. Conductance shift curves demonstrate that the suspended graphene sensors functionalized with specific anti-PSA antibodies as bioreceptor are capable of detecting prostate specific antigen down to 0.4 fg/ml (11 aM), at least one order of magnitude lower than unsuspended devices. The noise spectra analysis confirms the lower level of $1/f$ noise in suspended graphene devices. Carbon nanotube sensor under the same conditions of design, manufacture, and measurement are implemented to compare with graphene devices, showing the prominent advantages of graphene as a sensing material.

1. Introduction

Recently, graphene is attracting tremendous interests due to its unique structural, electrical, chemical, and mechanical properties (Geim and Novoselov, 2007; Novoselov et al., 2004; Geim, 2009). Graphene, a two-dimensional monolayer of sp^2-bonded carbon atoms, exhibits exceptional high sensitivity through its crystal lattice, which tends to screen charge fluctuations more than one-dimensional systems such as carbon nanotubes (Robinson et al., 2008). With rational physical and/or chemical modification, graphene-based sensors are capable of detecting many types of molecules and ions (He et al., 2010a,b; Ohno et al., 2009). The charge transfer induced by adsorption of atoms or molecules on the graphene surface, resulting in the drift of the graphene conductance (Schedin et al., 2007; Hwang et al., 2007). Graphene has been proposed to hold great potentials for sensitive and label-free detection of chemical/biological species (Fowler et al., 2009; Wang et al., 2009). To date, research on graphene has been focused exclusively on graphene sensors anchored on substrates. Any uncontrolled and random perturbations at the interface and on the substrate would lead to significant device current fluctuations and contribute to the electrical flicker noise known as low-frequency $1/f$ noise, which will attenuate the sensitivity, especially in the extremely low concentration situations (Lin et al., 2006).

Cancer markers are molecules occurring in blood or tissue, which are associated with cancer and whose measurement or identification is elucidated very critical and efficient in disease prediction, diagnosis, and monitoring (Zhong et al., 2010; Lilja et al., 2008; Etzioni et al., 2003). The prevailing biosensor protocols for detection of cancer markers include the enzyme linked immunosorbent assay (ELISA) (Lu et al., 2009; Yu et al., 2006), surface plasmon resonance (SPR) (Lin and Ju, 2005; Campagnolo et al., 2004), nanomaterial sensor array (Nam et al., 2003; Xue and Cui, 2008; Zheng et al., 2005), etc. In the meanwhile, the clinical utility of protein biomarker to discriminate health and disease requires the capability to measure extremely low concentration proteins, which is also especially important to understand cellular processes and to search for new protein biomarkers (Tessler et al., 2009; Todd et al., 2007). However, the detection limits of these methods have lagged behind the requirements for clinical utility and research. To overcome the hurdles of the previous detection methods, the signal to noise ratio must be improved because the electrical flicker noise is ubiquitous in solid state electronic devices. Therefore, using suspended self-assembly of graphene composites, an ultra-sensitive and label free cancer marker biosensor was synthesized for detecting of prostate specific antigen (PSA) in a large detection range from 0.4 fg/ml to 4 μg/ml, exceeding lots of the existing detection studies (Zhong et al., 2010; Yu et al., 2006; Lin and Ju, 2005; Campagnolo et al., 2004; Nam et al., 2003; Xue and Cui, 2008; Zheng et al., 2005). The noise density spectrum demonstrates that performance improvement of self-assembled graphene devices by strongly suspending the $1/f$ noise in the low frequency regime. In addition, a

* Corresponding author. Tel.: +1 612 626 1636.
E-mail address: tcui@me.umn.edu (T. Cui).

0956-5663/$ – see front matter © 2011 Elsevier B.V. All rights reserved.
doi:10.1016/j.bios.2011.09.046

carbon nanotube (CNT) based biosensor was characterized under the same design, fabrication, and measurement conditions in suspended states, demonstrating that graphene is superior to CNT with respect to the sensing detection limit.

2. Experiments

2.1. Materials

Research grade graphene (PureSheets^{TM}, 0.25 mg/ml) and carbon nanotube suspension solution (PureTube^{TM}, 0.25 mg/ml) were purchased from Nanointegris Inc. The polyelectrolytes were poly(diallyldiamine chloride) (PDDA, 1.5 wt%, Sigma–Aldrich Inc.) and poly(styrene sulfonate) (PSS, 0.3 wt%, Sigma–Aldrich Inc.), with an addition of 0.5 M sodium chloride to enhance the ion strength. 0.1% poly-L-lysine (PLL) was received from Sigma–Aldrich Inc. without further treatments. PSA capture antibody solution was purchased from BioCheck Inc., and prepared by a dilution into PBS (Dulbecco's phosphate buffered saline, Invitrogen Inc.) to a concentration of 10 μg/ml. The PSA was purchased from EMD Chemicals Inc., and also prepared by a dilution into PBS to different concentrations. 3% bovine serum albumin (BSA) was purchased from Sigma–Aldrich Inc. The normal rabbit immunoglobulin G (IgG) (sc-2027) and goat anti-rabbit IgG (sc-3836) were received from Santa Cruz Biotechnology Inc.

2.2. Sensor fabrication

Microfabrication was utilized to build the structure, and layer-by-layer (LbL) self-assembly method was used to deposit the graphene (Supplementary Fig. 1). First, graphene nanocomposite layers were LbL self-assembled on a clean silicon wafer with SiO_2 300 nm thick. The substrate was immersed into the charged suspensions with a sequence of [PDDA (10 min) + PSS (10 min)]$_2$ + [PDDA (10 min) + graphene suspension (20 min)]$_5$. Subsequently, the LbL self-assembled graphene was patterned to ribbons by oxygen plasma etching with STS etcher (Model 320, 30 s). Next, chromium/gold layers with 50/200 nm thick were deposited on the substrate by an AJA sputter system (Model ATC 2000). After the patterning of metal layers at the two ends of graphene ribbons, they play the roles of clamps and electrodes for the biosensors. Then, the unsuspended graphene biosensors were fabricated. In order to obtain suspended graphene biosensors, the SiO_2 layer 300 nm thick underneath graphene ribbons was etched away by buffered HF (BOE 10:1) for 5 min. Finally, the self-assembled graphene was released by SF_6 dry etching of the silicon underneath with STS etcher (Model 320, 10 min). According to the dry etching rate and the etching time, the gap under the graphene layer is about 10 μm.

After the suspension of graphene, the biosensor was functionalized by immobilization of capture antibody on the surface. Due to the surface tension of water, the surface modification process of graphene was executed in the aqueous solution all the time to keep the suspension state of graphene (Supplementary Fig. 4). A suspended graphene sensor was first immersed into a 0.1% PLL aqueous solution positive charged for 1 h, which enhanced the immobilization of antibodies. Next, the graphene sensor was incubated for overnight at 4 °C in PSA capture antibody solution at a concentration of 10 μg/ml. The sensor was immersed in a PBS solution for 10 min to rinse the biosensors. Then, the sensor was incubated in a 3% BSA blocking solution at room temperature for 5 h to block nonspecific binding sites. After repeating the rinsing step, the label free sensor was ready for testing.

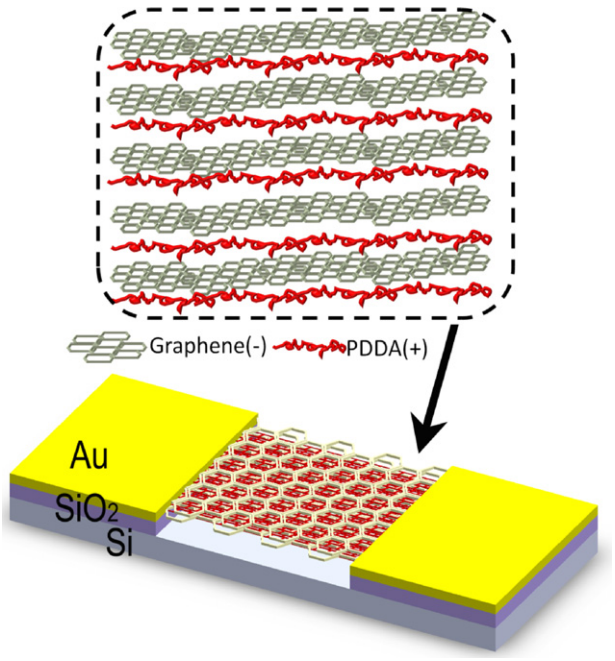

Fig. 1. Sketch of suspended LbL self-assembled graphene sensor structure, the self-assembled graphene serves as the conducting channel bridging the electrodes of a biosensor. Five bilayers of PDDA/graphene are synthesized by alternatively immersing the substrate into negative charged graphene suspensions and positive charged PDDA solutions. Suspended structure was released by dry etching of a silicon substrate.

2.3. Electrical testing

The conductance shifts of graphene devices were monitored using Agilent Data Logger (34970A, Agilent Inc.). The noise spectra of biosensors were measured in a DC mode, where 30 mV bias voltage was applied by analog outputs of a Wavetek 164 (Tucker Electronics). Data was acquired at a frequency of 10 kHz by TDS 2024B (Tektronix Inc.).

3. Results and discussion

3.1. Characterization of layer-by-layer self-assembled graphene

Nowadays, chemists have reported that micromechanical exfoliation and chemical methods are possible to generate high quality graphene flakes (Levendorf et al., 2009; Li et al., 2008). Comparing with those complex graphene generation processes, another low cost choice is to use LbL self-assembly technique to form large scale graphene nanocomposites as a sensing material. LbL self-assembly is a versatile and simple technique for fabrication of ultra thin films by alternately adsorbing oppositely charged materials on a substrate. Materials used for this purpose include polyelectrolytes, proteins, and DNA (Hua et al., 2002). As shown in Fig. 1, the suspended graphene has a structural layer of (polymer/graphene)$_5$ with metal connections on both ends. This is easily attained by immersing the substrate alternatively into charged graphene suspensions and polyions, followed by HF buffer etching and SF_6 dry etching. The zeta potential of the graphene nanoplatelets is −42.61 mV at pH 7, determined by 90Plus/BI-MAS (Brookhaven Instruments Corp.). The thickness and resistance of 5 bilayers of a self-assembled graphene film are 45 ± 5 nm and 0.9 ± 0.01 kΩ, respectively, characterized by surface profiler P16 and Agilent data logger (34970A, Agilent Inc.).

The suspended LbL self-assembled graphene was inspected by scanning electron microscope (SEM). Tilted SEM images of the

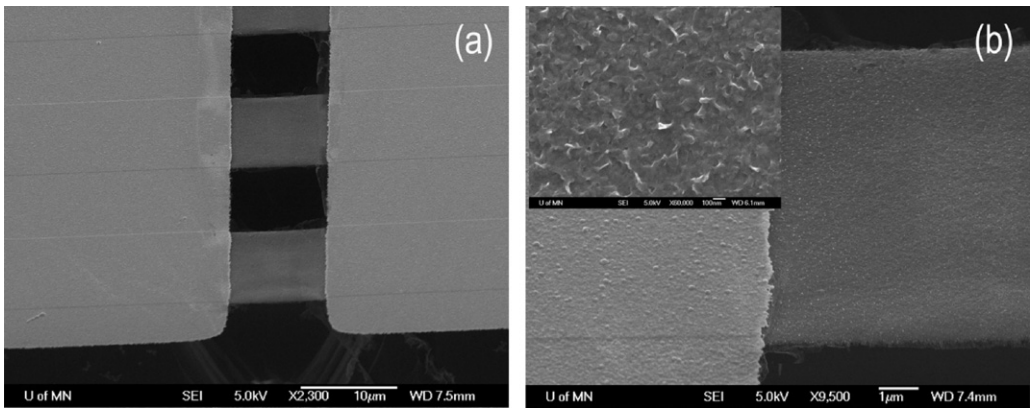

Fig. 2. (a) 45° tilted SEM image of the suspended graphene beam array. The channel length is 10 μm, and the width of the graphene beam is 10 μm. (b) Anchor part of the beam demonstrates the well fixed ends of the graphene beam. Inset: high magnitude of SEM image of LbL self-assembled graphene displays its porous defoliation surface profile details. The average graphene nanoplatelet is about 100 nm × 100 nm.

suspended graphene beam array are shown in Fig. 2a. Especially, an anchor part of the graphene beam is presented in Fig. 2b, showing the firmly fixed suspended graphene beam end. The intensively amplified image presents the defoliation of LbL self-assembled graphene surface profile. The average size of graphene nanoplatelet is about 100 nm × 100 nm (inset of Fig. 2b).

3.2. PSA detection by suspended graphene cancer sensors

Fig. 3 illustrates the overall design of self-assembled graphene based cancer sensors. After surface modification of cancer sensors, the anti-PSA was immobilized on the LbL self-assembled graphene nanocomposites, and the sensor was blocked with bovine serum albumin (BSA). Given that the conductance of graphene is determined by the charge carrier density and mobility, it is evident that changes in density and/or mobility of charge carriers must be responsive when molecules or ions are absorbed by graphene (Schedin et al., 2007; Hwang et al., 2007). The equation, $\sigma = nq\nu$ can show the relationship clearly, where σ is conductance, n is carrier density, q is charge per carrier, and ν is the carrier mobility. Therefore, the conductance of the graphene based biosensor modified with the PSA capture antibody shifts as the concentration change of PSA solutions. Electronic measurements of the suspended graphene cancer sensor reveal its improved detection limit. By suspending, the charge traps at the interface and in the oxide, which act as external scattering centers and degrade transport properties, are decreased greatly (Ratinac et al., 2010). Moreover, the porous defoliation profile of self-assembled graphene promises more exposure to proteins, providing the greatest sensing area per unit volume.

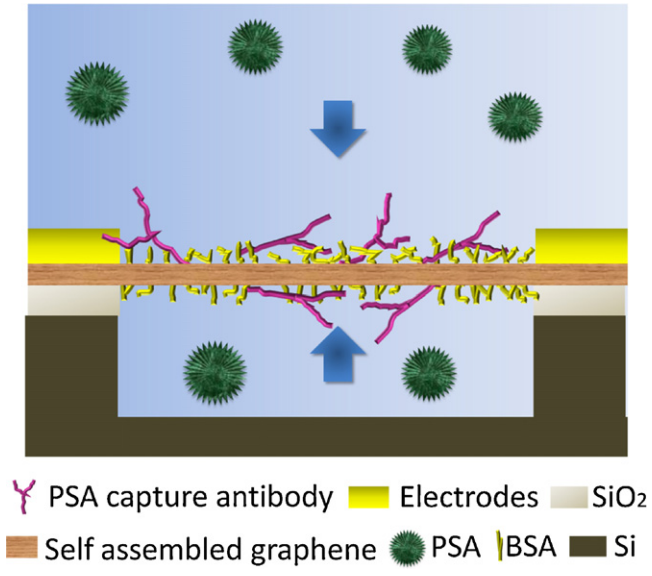

Fig. 3. Schematic illustration of immunoreaction between PSA capture antibodies and target protein PSA. Blocking solution BSA is introduced to enhance the specificity of the biosensor. After graphene biosensor modified by capture antibodies encounters the PSA solution, the immunoreaction will take place at both sides of the suspended graphene, and the conductance of graphene changes due to the absorption of PSA on the surface of the graphene.

The label free suspended graphene cancer sensor was characterized by measuring conductance with alternate different concentrations of PSA solutions prepared by PBS. Upon the introduction of PSA solution, the sensor resistance went down, meaning that the conductance of the sensor increased. Due to the stickiness of water and surface force in micro-scale, all the detection experiments were processed in an aqueous environment to avoid the collapse of suspended structure of self-assembled graphene. As is shown in Fig. 4a, the normalized conductance of graphene raises with the increase of PSA concentration from 0.4 fg/ml to 4 μg/ml. In comparison, the unsuspended graphene cancer sensor manufactured under the same conditions was conducted to compare with suspended sensors on the detection limits. It is clear to see that suspended graphene sensors were capable of detecting the shifts from 0.4 fg/ml to 4 fg/ml, but unsuspended devices were not. As is shown in Fig. 4b, the conductance versus time measurements recorded on the graphene biosensor in both suspended and unsuspended situations further confirm the trend in a real-time detection, indicating that the suspension is capable of enhancing the performance of detecting limits. By measuring the real-time response of graphene sensors, it is noticed that their conductance were almost the same before inducing 4 pg/ml PSA solution in unsuspended devices, and the signal was very fluctuating. After suspending the graphene, the "step" response of the device has a much more stable signal. These interesting results are determined by the strong decrease of electrical noises in suspended graphene, comparing with the unsuspended one. The non-specific reaction of normal rabbit IgG was also implemented to prove the specificity of this biosensor functionalized with PSA capture antibodies (Fig. 4b). In addition, different concentrations of PSA were delivered to suspended graphene sensors without modification and with goat anti-rabbit IgG modified, respectively (Lu et al., 2009) (Supplementary Fig. 2). The conductance of graphene sensor without any modification kept constant, demonstrating that the PSA was bound to the specific antibody and not directly to the surface.

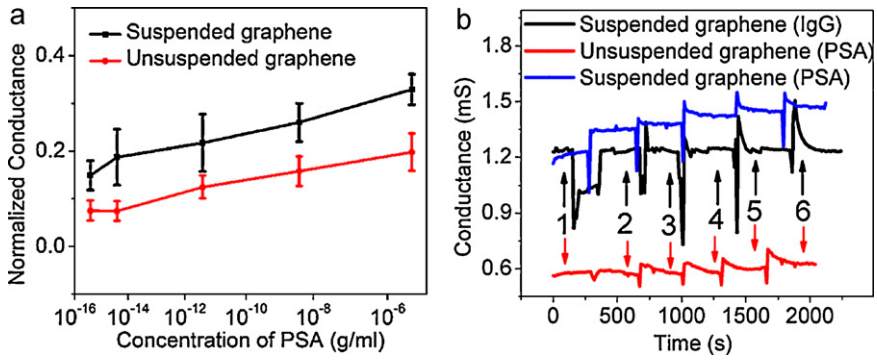

Fig. 4. (a) Shift in normalized conductance versus PSA concentration for suspended and unsuspended graphene sensors. The detection limit of suspended device can reach down to 0.4 fg/ml. The conductance was extracted from the stable region of the real time conductance measurement curve. After delivering the PSA solution each time, it takes several minutes for the conductance to get stabilized, allowing sufficient inmunoreaction and avoiding the disturbance generated by the delivery of PSA solutions. For a clear readout from different batches of samples, normalized conductance was introduced. Conductance under the condition of PBS without PSA was used as an initial conductance, G_0, and other conductance tested under different concentrations subtracted G_0 to get ΔG. Normalized conductance represented as $\Delta G/G_0$. The error bar is established from 5 samples. (b) Conductance versus time for suspended and unsuspended graphene with different concentrations of PSA solutions introduced: (1) PBS contains no PSA, (2) 0.4 fg/ml, (3) 4 fg/ml, (4) 4 pg/ml, (5) 4 ng/ml, and (6) 4 μg/ml. The results reconfirm that the detection limit of suspended graphene sensor is much better than unsuspended devices. Normal rabbit IgG were also delivered to suspended graphene sensor functionalized with PSA capture antibodies under the same experimental conditions, and the conductance of graphene sensor kept constant, demonstrating the specificity of suspended graphene biosensor.

The graphene biosensor response can be explained by the strong interaction between PSA and its bio-receptors. However, further research is required to reveal the mechanism. The conductance of graphene sensor with goat anti-rabbit IgG modified also kept constant, demonstrating the specificity of this biosensor on the other hand.

The detection limit of a sensor that can be processed is ultimately determined by its signal-to-noise ratio. If the input signal and sensor structure are constant, the output signal is supposed to be more stable and sensitive due to the lower $1/f$ noise. Thus the noise spectra of suspended and unsuspended graphene devices were further investigated under the same experimental conditions, and concentrated on low-frequency (below 1 kHz) noise reported to be dominant in limiting performance of nanodevices (Lin and Avouris, 2008). The current power spectra can be expressed as $S_I = AI^2 f^{\beta}$, where S_I is the noise power density, I is the current, f is the frequency, A is defined as the $1/f$ noise amplitude, and β is the frequency exponent with a value close to -1 (Lin et al., 2006). Fig. 5 shows the noise power spectrum S_I, normalized by the mean square of current, for both suspended and unsuspended graphene biosensors as a function of frequency. The noise level of the self-assembled graphene devices is decreased by one order of magnitude from the unsuspended state to the suspended state. It was reported that trapped charges at the interface and in the substrate degrade transport characteristics of a single-layer graphene (Du et al., 2008; Bolotin et al., 2008; Liu et al., 2009), which exhibit the effect in our experiment results. In addition, due to the self-assembly technique and polymers, the surface profile of the graphene layers shows great porous topography, more suitable to decorate capture proteins, providing the greatest sensing surface area per unit volume. Moreover, the suspended structure exposing to both sides of the graphene layers doubles the sensing area comparing with the similar pattern in an unsuspended structure, which is helpful to enhance the output signal.

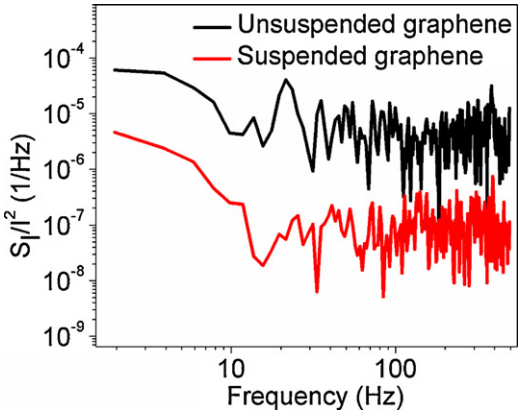

Fig. 5. Normalized noise power spectrum of the graphene biosensor was characterized. Comparison of graphene's noise power spectra with and without suspension situation shows lower level of $1/f$ noise in suspended devices.

3.3. PSA detection by suspended CNT cancer sensor

The self-assembled CNT sensor manufactured under the same conditions as the self-assembled graphene sensor was conducted to compare with graphene sensors on the detection limits. As is shown in Fig. 6, real-time results indicate that the CNT sensor was only capable of detecting PSA at a concentration of 4 pg/ml, much less sensitive than the graphene sensor. The difference of the detection limits between graphene and CNT sensor may be explained by the intrinsic $1/f$ noise (Yang et al., 2010). In the case of CNT, such fluctuation noise can arise from trapped charges in the antibodies

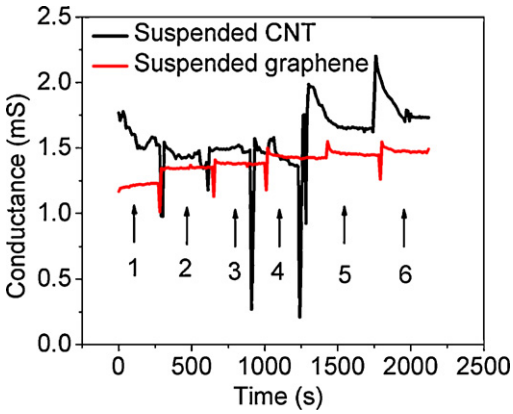

Fig. 6. Conductance versus time testing for suspended graphene and CNT biosensors with different PSA concentrations: (1) PBS contains no PSA, (2) 0.4 fg/ml, (3) 4 fg/ml, (4) 4 pg/ml, (5) 4 ng/ml, and (6) 4 μg/ml. The results show that the detection limit of suspended graphene sensor is down to 0.4 fg/ml, compared with the suspended CNT sensor with a detection limit of 4 pg/ml.

(Lin et al., 2006; Ishigami et al., 2006) or the presence of defects within self-assembled tube networks. Interestingly, an effective screening of charge fluctuations from external impurity charges is identified in graphene due to its high quality of crystal lattice and two-dimensional honeycomb structure (Robinson et al., 2008). Such screening effects may explain the reduction of an electrical noise level indicated by the normalized noise power spectrum of suspended graphene and CNT sensors (Supplementary Fig. 3).

4. Conclusion

Suspended LbL self-assembled graphene was demonstrated to provide a simple and effective way to synthesize ultra-sensitive and label free sensors to detect cancer markers with a detection limit down to 0.4 fg/ml. The suspended graphene sensors were highly responsive to the low concentration of PSA, exhibiting lower detection limits than unsuspended graphene devices. The sensing response could be attributed mainly to the strongly suppression of electrical flicker noise through the suspension of graphene. The noise spectra analysis further indicated the lower level of $1/f$ noise in suspended graphene devices. The CNT biosensors under the same design and fabrication procedures were also compared with the graphene devices in suspended states, revealing that graphene is superior to CNT for the low detection limit applications.

Acknowledgements

The authors acknowledge the assistance of fabrication and characterization from Nanofabrication Center and the Characterization Facility at the University of Minnesota.

Appendix A. Supplementary data

Supplementary data associated with this article can be found, in the online version, at doi:10.1016/j.bios.2011.09.046.

References

Bolotin, K.I., Sikes, K.J., Jiang, Z., Klim, M., Fudenberg, G., Hone, J., Kim, P., Stormer, H.L., 2008. Solid State Commun. 146, 351–355.
Campagnolo, C., Meyersc, K.J., Ryand, T., Atkinsond, R.C., Chene, Y., Scanlanf, M.J., Ritterf, G., Oldf, L.J., Bat, C.A., 2004. J. Biochem. Biophys. Methods 61, 283–298.
Du, X., Skachko, I., Barker, A., Andrei, E.Y., 2008. Nat. Nanotechnol. 3, 491–495.
Etzioni, R., Urban, N., Ramsey, S., McIntosh, M., Schwartz, S., Reid, B., Radich, J., Anderson, G., Hartwell, L., 2003. Nat. Rev. Cancer 3, 243–253.
Fowler, J.D., Allen, M.J., Tung, V.C., Yang, Y., Kaner, R.B., Weiller, B.H., 2009. ACS Nano 3, 301–306.
Geim, A.K., 2009. Science 324, 1530–1534.
Geim, A.K., Novoselov, K.S., 2007. Nat. Mater. 6, 183–191.
He, Q., Sudibya, H.G., Yin, Z., Wu, S., Li, H., Boey, F., Huang, W., Chen, P., Zhang, H., 2010a. ACS Nano 4, 3201–3208.
He, S., Song, B., Li, D., Zhu, C., Qi, W., Wen, Y., Wang, L., Song, S., Fang, H., Fan, C., 2010b. Adv. Funct. Mater. 20, 453–459.
Hua, F., Shi, J., Lvov, Y., Cui, T., 2002. Nano Lett. 2, 1219–1222.
Hwang, E.H., Adam, S., Das Sarma, S., 2007. Phys. Rev. B 76, 195421.
Ishigami, M., Chen, J.H., Williams, E.D., Tobias, D., Chen, Y.F., Fuhrer, M.S., 2006. Appl. Phys. Lett. 88, 203116.
Levendorf, M.P., Ruiz-Vargas, C.S., Garg, S., Park, J., 2009. Nano Lett. 9, 4479–4483.
Li, X., Zhang, G., Bai, X., Sun, X., Wang, X., Wang, E., Dai, H., 2008. Nat. Nanotechnol. 3, 538–542.
Lilja, H., Ulmert, D., Vickers, A.J., 2008. Nat. Rev. Cancer 8, 268–278.
Lin, J., Ju, H., 2005. Biosens. Bioelectron. 20, 1461–1470.
Lin, Y., Avouris, P., 2008. Nano Lett. 8, 2119–2125.
Lin, Y., Appenzeller, J., Knoch, J., Chen, Z., Avouris, P., 2006. Nano Lett. 6, 930–936.
Liu, G., Stillman, W., Rumyantsev, S., Shao, Q., Shur, M., Balandin, A.A., 2009. Appl. Phys. Lett. 95, 033103.
Lu, M., Lee, D., Xue, W., Cui, T., 2009. Sens. Actuators A 150, 280–285.
Nam, J., Thaxton, C.S., Mirkin, C.A., 2003. Science 301, 1884–1886.
Novoselov, K.S., Geim, A.K., Morozov, S.V., Jiang, D., Zhang, Y., Dubonos, S.V., Grigorieva, I.V., Firsov, A.A., 2004. Science 306, 666–669.
Ohno, Y., Maehashi, K., Yamashiro, Y., Matsumoto, K., 2009. Nano Lett. 9, 3318–3322.
Ratinac, K., Yang, W., Ringer, S., Braet, F., 2010. Environ. Sci. Technol. 44, 1167.
Robinson, J.T., Perkins, F.K., Snow, E.S., Wei, Z.Q., Sheehan, P.E., 2008. Nano Lett. 8, 3137–3140.
Schedin, F., Geim, A.K., Morozov, S.V., Hill, E.W., Blake, P., Katsnelson, M.I., Novoselov, K.S., 2007. Nat. Mater. 6, 652–655.
Tessler, L.A., Reifenberger, J.G., Mitra, R.D., 2009. Anal. Chem. 81, 7141–7148.
Todd, J., Freese, B., Lu, A., Held, D., Morey, J., Livingston, R., Goix, P., 2007. Clin. Chem. 53, 1990–1995.
Wang, Z., Zhou, X., Zhang, J., Boey, F., Zhang, H., 2009. J. Phys. Chem. C 113, 14071–14075.
Xue, W., Cui, T., 2008. Sens. Actuators B 134, 981–987.
Yang, W., Ratinac, K., Ringer, S., Thordarson, P., Gooding, J., Braet, F., 2010. Angew. Chem. Int. Ed. 49, 2114–2138.
Yu, X., Munge, B., Patel, V., Jensen, G., Bhirde, A., Gong, J.D., Kim, S.N., Gillespie, J., Gutkind, J.S., Papadimitrakopoulos, F., Rusling, J.F., 2006. J. Am. Chem. Soc. 128, 11199–11205.
Zheng, G., Patolsky, F., Cui, Y., Wang, W.U., Lieber, C.M., 2005. Nat. Biotechnol. 23, 1294–1301.
Zhong, Z., Wu, W., Wang, D., Wang, D., Shan, J., Qing, Y., Zhang, Z., 2010. Biosens. Bioelectron. 25, 2379–2383.